NANO LETTERS

Communication

Therapeutic Delivery to the Brain via the Lymphatic Vasculature

Pengfei Zhao, Zhicheng Le, Lixin Liu, and Yongming Chen

Nano Lett., **Just Accepted Manuscript** • DOI: 10.1021/acs.nanolett.0c01806 • Publication Date (Web): 08 Jun 2020

Therapeutic Delivery to the Brain via the Lymphatic Vasculature

Pengfei Zhao[†], Zhicheng Le[†], Lixin Liu[†,], Yongming Chen[†,]**

[†] School of Materials Science and Engineering, MOE Key Laboratory of Polymeric Composite and Functional Materials (PCFM), Sun Yat-sen University, Guangzhou, 510275, China

KEYWORDS: Brain delivery, Cerebral lymphatic vasculature, Nanoparticles, Orthotopic glioblastoma, Photodynamic therapy

ABSTRACT: Targeted delivery of therapeutics to disease sites has been one of the biggest challenges in medicine as it determines treatment efficacy of virtually all chemical and biological drugs. Furthermore, it is particularly difficult to achieve for diseases in the brain because of an additional barrier compared to other organs, the blood-brain barrier (BBB). Here, we report a new mechanism for drug delivery to brain, nanoparticle-mediated transport through the newly discovered brain lymphatic vasculatures, bypassing the BBB and other issues associated with conventional intravenous (*i.v.*) administration. Using indocyanine green (ICG)-loaded PLGA nanoparticles as a model, we show that drug uptake in the brain by subcutaneous (*s.c.*) injection at neck near local lymph node is 44-fold higher than the *i.v.* route, resulting in effective treatment

of glioblastoma in mice by photodynamic therapy. These findings will open a new paradigm for the treatment of a variety of diseases in the brain.

INTRODUCTION

Central nervous system (CNS) diseases such as glioblastoma and the neural degeneration are among the deadliest and costliest with the highest degree of patient suffering. New chemical and biological therapeutics tested effective *in vitro* rarely advance to the clinical stages, because therapeutics delivered through the conventional routes (e.g., *i.v.* administration) cannot effectively cross the transport barriers, in particular the BBB, a natural, robust mechanism that strictly regulates mass exchange between the bloodstream and brain tissues.[1,2] To address this challenge, several strategies aiming at disrupting the BBB, such as the use of virally derived peptides and toxins, have been developed to improve the brain delivery efficiency.[3-5] However, breaching the integrity of the BBB raises major safety concerns, particularly for repeated treatments.[6] In addition, the majority of drugs administered intravenously do not survive the first-pass metabolism in the liver, further reducing their bioavailability.

To address this fundamental difficulty in getting therapeutics into the brain, we hypothesized that they can be delivered via the lymphatic system, a pivotal component for vascular transport of the body and homeostasis.[7] Driven by the slow interstitial fluid flow from the vascular capillaries, lymphatic vessels offer a channel to transport macromolecules and particles into tissue interstitium.[8] A recent stunning discovery by Louveau *et al.* revealed functional lymphatic vasculature lining the dural sinuses and connecting to deep cervical lymph nodes (dCLNs).[9-11] These conduits bridge the cervical lymph nodes (CLNs) and cerebral spinal fluid (CSF) for exchange of fluids and immune cells.[1] This discovery not only changed the central dogma of

neuroimmunology but also had important implications for the management of major neurological disorders. Due to the easy access of the CLNs to the lymphatic vasculature, we set out to study whether properly formulated nanotherapeutics can be effectively delivered to the brain through this brain lymphatic vasculature following subcutaneous (*s.c.*) injection, thus bypassing the aforementioned limitations of the *i.v.* administration route.

RESULTS AND DISCUSSION

Preparation and characterizations of model nanoparticles. To test this hypothesis, we selected ICG as a model therapeutic, as it is the only FDA-approved near infrared (NIR) fluorophore for *in vivo* imaging and is an efficient photosensitizer for photodynamic therapy (PDT). Therefore, *in vivo* imaging and a model treatment experiment can be performed using the same molecule. ICG-loaded poly(D,L-lactide-*co*-glycolide) (PLGA) nanoparticles were prepared using the flash nanoprecipitation technique, a kinetically controlled process capable of making nanoparticles with tight size control in a scalable manner.[12,13] Because lymphatic system-based drug delivery is known for size dependence,[14,15] three sets of nanoparticles were prepared with sizes of 45.9 ± 0.9 nm (NP-1), 113.2 ± 4.1 nm (NP-2), and 180.9 ± 3.1 nm (NP-3) and narrow size distribution (PDI < 0.2). These nanoparticles have high ICG-loading levels (9.7–10.5%) (**Table S1 and Figure S1-S2**) and show a high colloidal stability in physiological medium due to the presence of Pluronic F68 (**Figure S3-S4**).

Cerebral lymphatic vasculature-mediated NP delivery into the brain. To evaluate the transport efficacy of the lymphatic-system and ICG biodistribution in the brain, the ICG-loaded nanoparticles were injected subcutaneously (*s.c.*) in the mouse neck near the superficial and deep cervical lymph nodes (sCLNs and dCLNs). NIR fluorescence was monitored by *ex vivo* imaging of mouse brain tissues at multiple time points. As shown in **Figure 1a-c and Figure S5**, ICG-

signal increases slowly and peaks at around 24 h post-administration. Quantitatively, free ICG dyes accumulated in the mouse brain at about 0.8% of the total injected dose at 24 h and were cleared by 48 h. The NP groups yielded significantly higher accumulation in brain parenchyma: NP-1 delivered the highest level, 8.8 ± 0.5% of the total dose in the brain, 11-fold higher than that of free ICG; while NP-2 and NP-3 reached 6.0 ± 0.5% and 3.8 ± 0.3%, respectively. This size-dependent transport and accumulation behavior is consistent with previous reports on nanoparticle-mediated lymphatic drainage for other organs[8]. In contrast, *i.v.* injections of the nanoparticles or free ICG dyes did not retain in the brain and only resulted in background level ICG (0.1-0.2%) in the brain (**Figure 1d, e and Figure S5**). To examine the general nanoparticle *in vivo* biodistribution, ICG fluorescence in other major organs was also analyzed at multiple time points (**Figure S6**). ICG accumulation in most organs (except the kidney) peaked around 24 h post *s.c.* injection, and gradually decreased to approximately 50% by 48 h (**Figure 1b, Figure S6**).

Two separate control experiments were also conducted to better understand this new route of delivery. First, NP-1 was *s.c.* injected near the mouse tail. 24 h post-injection, no appreciable fluorescence signals were detected in the mouse brain and CLNs, suggesting that the *s.c.* injection site was also crucial for NP brain delivery (**Figure S7**). Second, a meningeal lymphatic vessel (MLV)-ligated mouse model was developed by surgically cutting and ligating the lymphatic vessels to verify the impact of the cerebral lymphatic vasculature for effective NP delivery into the brain. As shown in **Figure S8**, NP-1 delivered into the brain was substantially reduced 24 h after *s.c.* administration, suggesting that NPs delivered into normal mouse brains were via the cerebral lymphatic vessels. Taken together, these results suggest that *s.c.* injection of optimized nanoparticle formulations near CLNs and their subsequent transport through the

lymphatic system can become a significantly better option than *i.v.* administration for drug delivery into the brain.

To study if the observation of nanoparticle accumulation in the brain is limited to PLGA particles, PEGylated superparamagnetic iron oxide nanoparticles (SPIOs) were administered the same way. 24 h post-injection, SPIOs also became visible in the brain parenchyma (**Figure S9, S10**). This result demonstrates that lymphatic vasculature-mediated brain delivery is a general approach for delivering small particles to the brain.

Mechanism of NP delivery into the brain via the lymphatic vasculature. To confirm the brain lymphatic vasculature-mediated delivery, particularly the initial drainage of nanoparticles from the injection site to nearby lymph nodes (LNs), CLNs and axillary LNs (ALNs) were excised and imaged at 24 h post-injection (**Figure 2a**). NP-1 was selected to compare with bare ICG because of its optimal delivery into the brain among the three NPs. As shown in **Figure 2a**, accumulations of NP-1 in both sets of LNs were significantly higher than free ICG, with the strongest fluorescence found in the CLNs. These results are somewhat expected because it is well established that small-molecule drainage from the interstitial space primarily occurs *via* the blood capillaries instead of lymphatic vessels because of faster (100s fold) flow rate; whereas macromolecules and nanoparticles preferentially enter the lymphatic circulation[8].

The fluorescence intensities of dCLNs were further quantified because they are connected to the meningeal lymphatic vessels lining the dural sinuses, and the drug concentration in dCLNs may directly impact its concentration in the brain[9]. ICG dosage accumulated in dCLNs measured at 16, 24, and 48 h post *s.c.* injection of NP-1 was 551 ± 55, 829 ± 94, and 713 ± 118 $ng \cdot mg^{-1}$, respectively (**Figure 2b**). Similar to *s.c.* delivery to other LNs,[16-18] small NPs moved through the interstitium and entered lymphatic vessels more efficiently than the free drug (**Figure S11**).

Fluorescence imaging of the meningeal lymphatic vessel directly connected to dCLNs at 24 h post-injection revealed strong ICG signals in the meningeal lymphatic vessels for NP-1 injection (**Figure 2c**).

Next, we measured ICG concentration in the CSF, which reflects the amount of drug accessible to the CNS.[19,20] Much higher ICG concentration in CSF at 24 h post-injection was detected for NP-1 group (6.2 ± 1.6 $\mu g \cdot mL^{-1}$), compared to free ICG (0.1 ± 1.3 $\mu g \cdot mL^{-1}$) (**Figure 2d**). To explore the mechanism of nanoparticle entry into the CSF, we investigated the distribution of NP-1 in mouse dCLNs 24 h post *s.c.* administration. As shown in **Figure 2e and f**, NP-1 mainly located inside cells, with 24.7% of dendritic cells (DCs), 19.0% of T lymphocytes and 38.0% of B lymphocytes in the dCLNs showing ICG signals. Although this result cannot rule out the possibility that nanoparticles can diffuse through the lymphatic vessels into the brain, it strongly suggests that NPs diffused continuously from the CLNs to lymphatic vessels and CSF piggybacking on immune cells.

***In vitro* photodynamic therapy effect of NP.** To demonstrate the utility of this new drug delivery mechanism, we tested the effectiveness of NP-1 (best-performing among the three NPs) for the treatment of glioblastoma in cells and mice as a model. Compared to free ICG, NP-1 after laser irradiation produced a higher level of reactive oxygen species (ROS), likely due to the protection and improved photostability offered by the nanoparticle carrier (**Figure 3a, b**).[21] Cellular uptake efficiency of NP-1 in rat C6 glioblastoma cells was 1.6-fold higher than free ICG (**Figure 3c**, **e)**. Accordingly, ROS generated intracellularly after laser irradiation (808 nm, 10 min, 120 J) was 2.4-fold higher than free ICG and slightly higher than the ROS inducer[22] (**Figure 3d**, **f, and Figure S12**), as a result of improved cell uptake. Furthermore, the higher ROS levels generated by NP-1 translated into higher photodynamic therapy (PDT) efficacy

under the same laser irradiation condition. Cell death approached 60% when free ICG was used at 40 μg·mL^{-1} (**Figure 3g**), whereas NP-1 enabled 76% cell death at an NP-1 dose equivalent to 20 μg·mL^{-1} ICG. These results indicate that NP-1 is significantly more effective than free dyes as PDT agents.

NP-1 biodistribution in glioblastoma-bearing mouse brain. Next, we compared brain delivery efficiencies of NP-1 and free ICG in a mouse model for early-stage orthotopic glioblastoma. 24 h post *s.c.* injection near the CLNs of tumor-bearing mice, NP-1 delivery yielded a 2.6-fold higher ICG signal than free ICG. Furthermore, it is interesting to note that the fluorescence in the tumor region was especially higher compared with the rest of the brain (**Figure 4a**), likely due to tumor-associated inflammations that attracted immune cells. Similar to mice without tumor implantation (**Figure 1a**), no apparent ICG signal was detected after *i.v.* injection of all three groups (**Figure 4a**).

PDT effect of NP-1 to orthotopic glioblastoma. We then generated an orthotopic glioblastoma mouse model by intracranial injection of 1×10^5 luciferase-expressing C6 cells per mouse, so that tumor sizes can be readily monitored by bioluminescence imaging *in vivo*. At day 6 following C6 implantation, NP-1 or free ICG was given to mice with detectable brain tumors. At 24 h following NP dosing, photo illumination (808 nm, 30 min, 360 J) was initiated. NP-1 induced significantly higher tumor cell apoptosis, evidently enhanced tumor suppression for 21 days followed by promoted mouse survival (50%) 45 days after cell inoculation (**Figure 4b**–**d**). In comparison, PDT induced by *s.c.* injected free ICG or *i.v.* injected ICG, NP-1 showed negligible curative effect (**Figure 4c**, **d**). No obvious tissue damage or dysfunction was observed following any of these treatments (**Figure S13**), indicating a high degree of biocompatibility of this therapeutic strategy. Thus, NP-mediated delivery through the CNS lymphatic vasculatures

represents a new and highly promising approach to deliver therapeutics into the brain for CNS diseases.

CONCLUSION

In conclusion, NP-mediated drug delivery into the brain via the cerebral lymphatic vasculature is demonstrated by utilizing ICG-loaded PLGA nanoparticles as a model. After *s.c.* administration of nanoparticles with optimized formulations near the CLNs, particles accumulate to dCLNs and continuously diffuse into lymphatic vessels and CSF via the transportation of immune cells, therefore leading to effective brain delivery bypassing BBB. Finally, retained NP-1 effectively suppresses orthotopic glioblastoma growth by photodynamic therapy. Lymphatic vasculature-mediated therapeutic delivery into the brain brings great opportunities for multiple brain disease treatments.

FIGURES

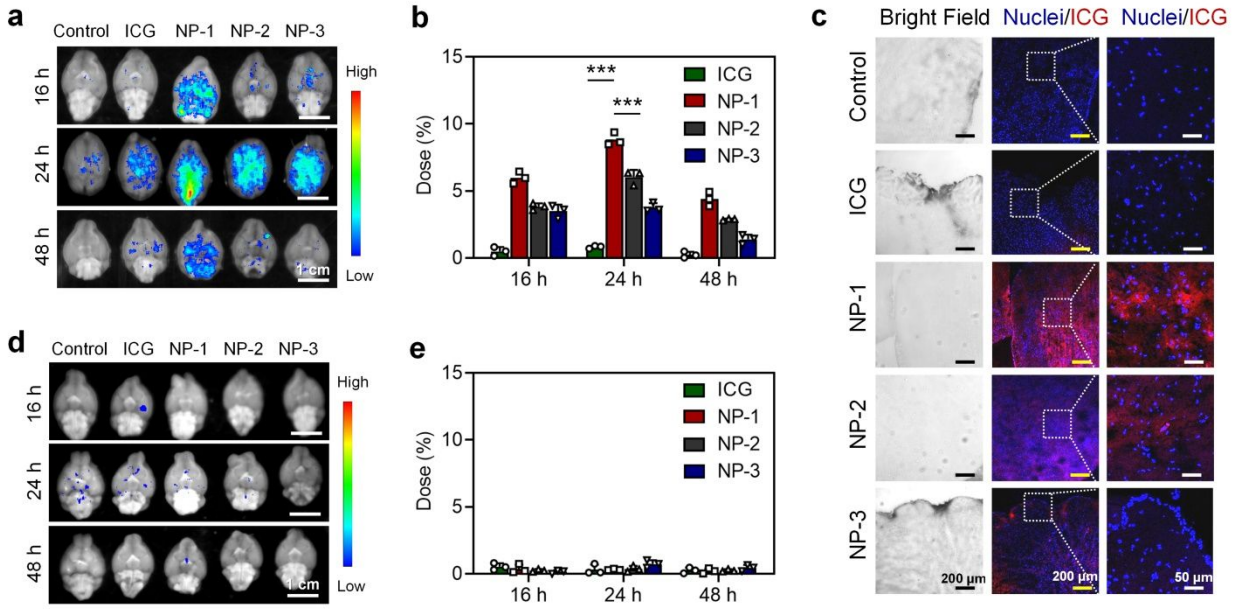

Figure 1. *In vivo* distribution of NPs in mouse brains. (a,b) Representative *ex vivo* fluorescence images of dissected mouse brains, and quantitative analysis of ICG and NP dose in the brain after *s.c.* administration of ICG or NPs. (***) $P < 0.001$ (n = 3, unpaired *t* test). (c) Biodistribution of ICG and NP in brain parenchyma 24 h post-injection. Frozen brain sections were counterstained with DAPI staining for the cell nuclei (blue). ICG and ICG-doped NPs were shown in red. (d,e) Fluorescence images of dissected mouse brains and quantitative analysis and ICG and NP dose in the brain after *i.v.* administration of ICG or NPs (n = 3).

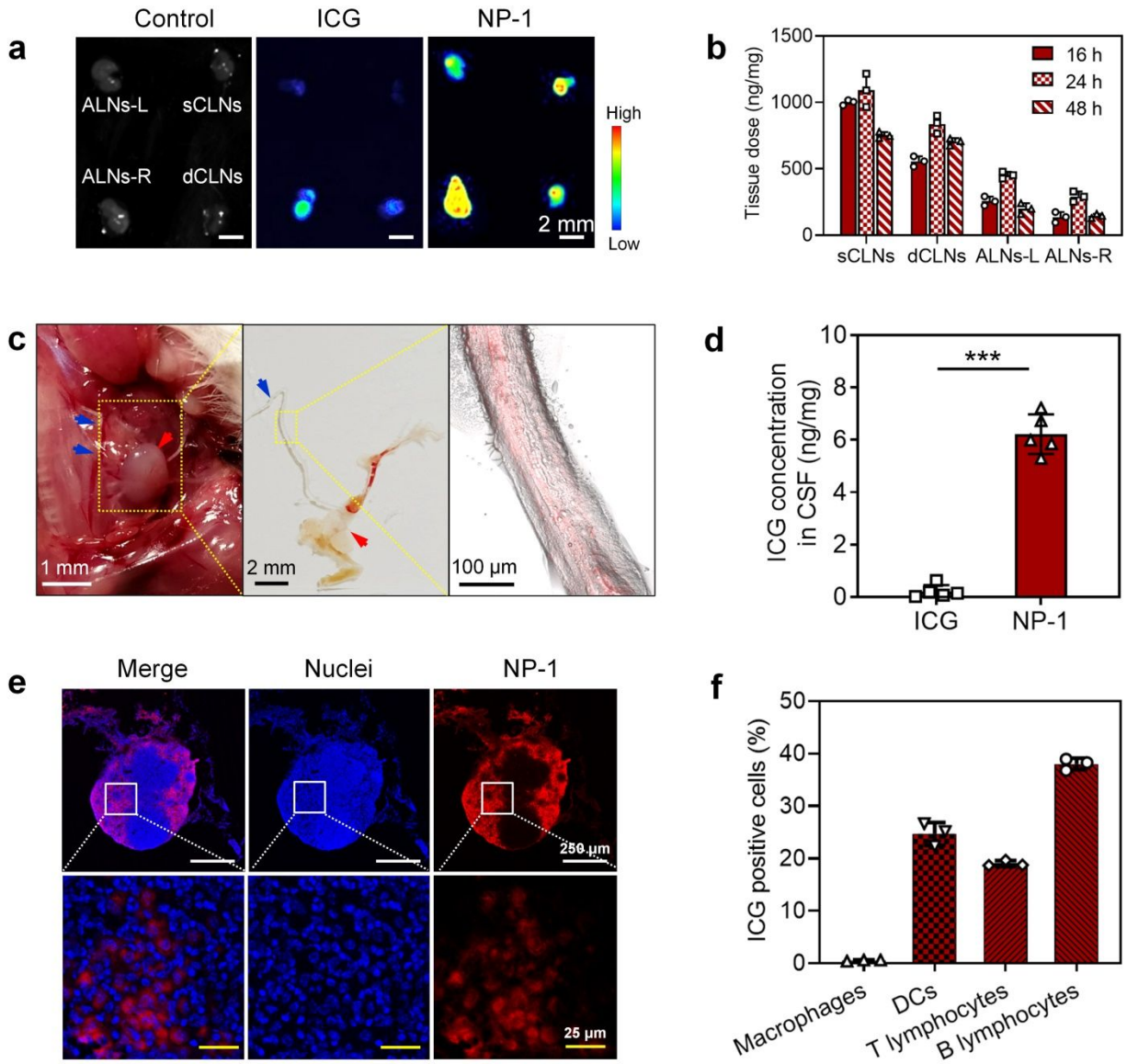

Figure 2. *In vivo* distribution of NP-1 in proximal LNs and meningeal lymphatic vessels. (a) Representative *ex vivo* fluorescence images of dissected mouse LNs 24 h after *s.c.* administration of PBS, ICG or NP-1 (L: left, R: right). (b) Quantitative NP-1 dosage in LNs 16, 24, and 48 h after *s.c.* administration. (c) NP-1 distribution in surgically isolated dCLNs (red arrowhead) and meningeal lymphatic vessels (blue arrowhead) 24 h post *s.c.* administration. ICG fluorescence was shown in red. (d) The quantitative concentration of ICG or NP-1 in mouse CSF 24 h after *s.c.* administration. (***) $P < 0.001$ (n = 5, unpaired *t* test). (e) NP-1 distribution in mouse

dCLNs 24 h after *s.c.* administration. Frozen LN sections were counterstained with DAPI staining for the Nuclei; (f) ICG-positive immune cells in dCLNs 24 h after *s.c.* administration of NP-1 (n = 3).

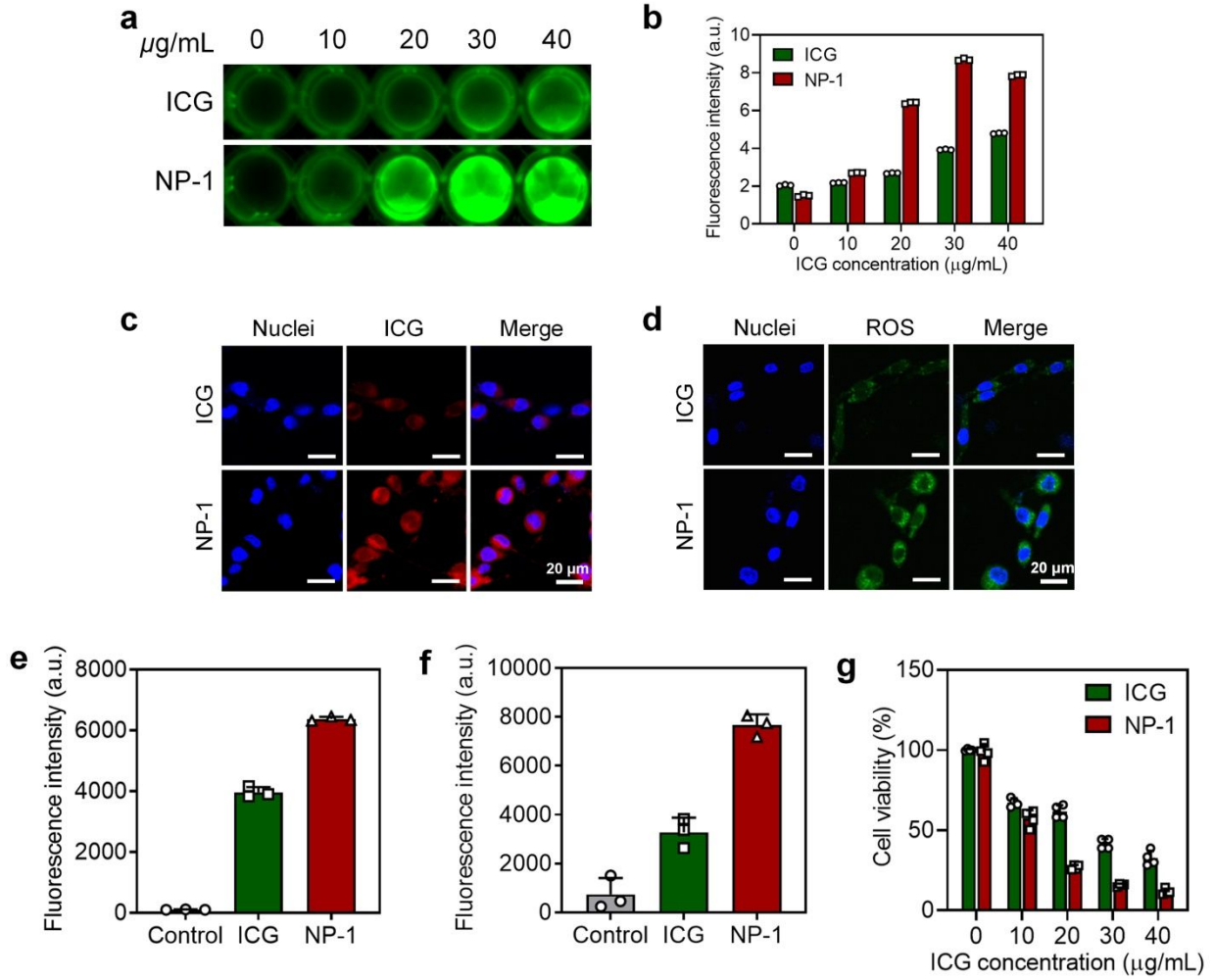

Figure 3. PDT *in vitro* using NP-1. (a) ROS generation of ICG and NP-1 aqueous solution after laser irradiation (808 nm, 10 min, 120 J). (b) Relative fluorescence intensities induced by the generated ROS (n = 3). (c) Glioblastoma cell uptake of ICG or NP-1 after 4 h incubation. (d) Intracellular ROS imaging after laser irradiation. (e) Quantification of cell uptake of ICG or NP-1 using flow cytometry (n = 3). (f) Quantification of intracellular ROS (n = 3). (g) *In vitro* PDT effect using ICG or NP-1 as photosensitizer in C6 cells (n = 4).

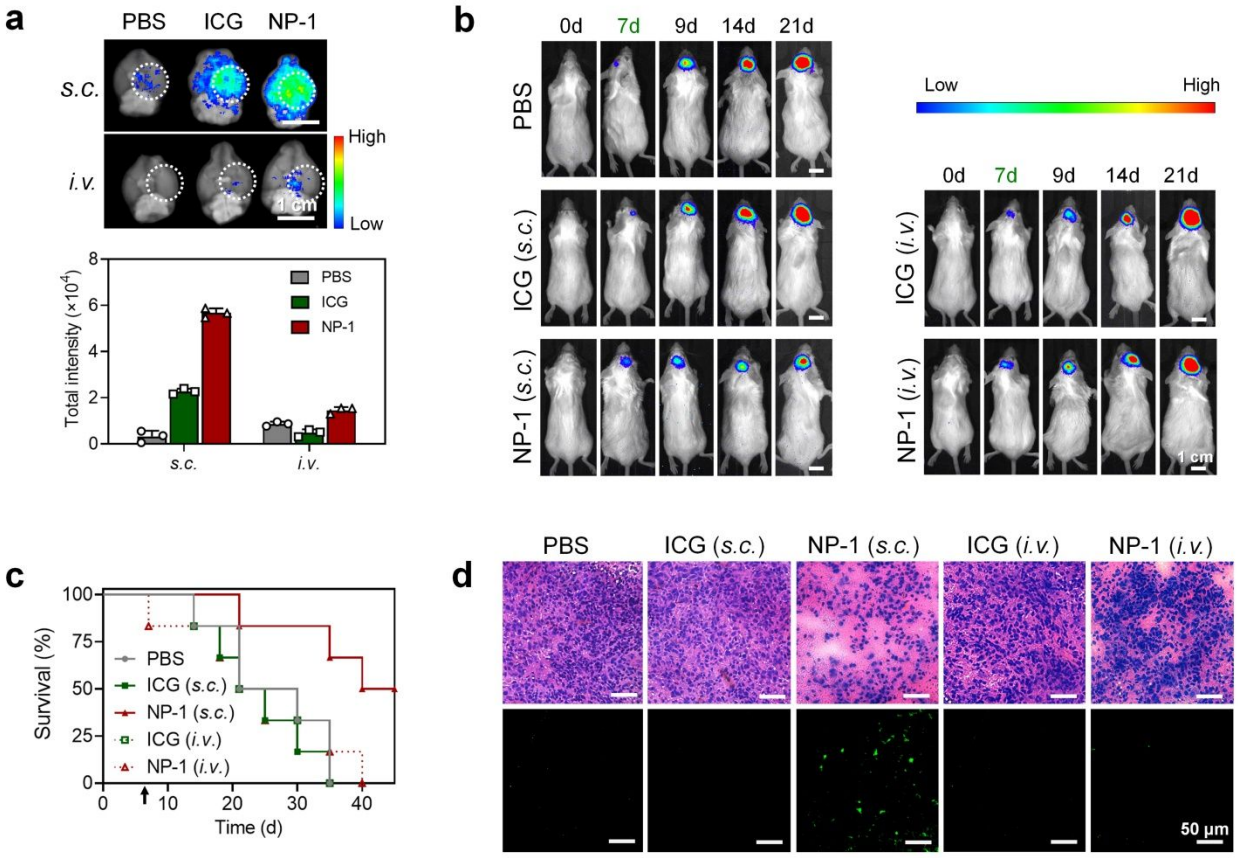

Figure 4. PDT effect of NP-1 in an orthotopic glioblastoma mouse model. (a) Distribution of bare ICG and NP-1 in the brain of glioblastoma-bearing mice 24 h post *s.c.* or *i.v.* injection. Dotted white circles outline tumor sites. (b) Representative bioluminescence images of mouse glioblastoma after different treatments. Images were acquired 10 min after injection of D-Luciferin. Mice were injected with PBS, ICG or NP-1 and irradiated with a NIR laser (808 nm, 30 min, 360 J) 24 h after injection. (c) Survival curves of tumor-bearing mice after different treatments. Black arrow indicates the time of laser irradiation (day 7) (n = 6). (d) Histological images and TUNEL assay (green fluorescence indicates apoptotic tumor cells) of glioblastoma tissue sections 48 h after PDT.

ASSOCIATED CONTENT

Supporting Information. The supporting information is available free online. Details for experimental methods, Figures S1-S12 and Table S1 are included (PDF).

AUTHOR INFORMATION

Corresponding Authors

Lixin Liu, liulixin@mail.sysu.edu.cn

Yongming Chen, chenym35@mail.sysu.edu.cn

Author Contributions

Pengfei Zhao and Zhicheng Le contributed equally to this work. All authors contributed to data analysis, reviewed and approved the manuscript.

Notes

The authors declare no competing financial interest.

ACKNOWLEDGMENT

This work is supported by the National Natural Science Foundation of China (No. 51533009), Guangdong Innovative and Entrepreneurial Research Team Program (No. 2013S086), and Science Foundation of Guangdong Province (No. 2014A030312018).

REFERENCES

1. Quail, D.F.; Joyce, J.A. The microenvironmental landscape of brain tumors. *Cancer Cell* **2017**, 31, 326–341.
2. Xue, J.W.; Zhao, Z.K.; Zhang, L.; Xue, L.J.; Shen, S.Y.; Wen, Y.J.; Wei, Z.Y.; Wang, L.; Kong, L.Y.; Sun, H.B.; Ping, Q.N.; Mo R.; Zhang, C. Neutrophil-mediated anticancer drug

delivery for suppression of postoperative malignant glioma recurrence. *Nat. Nanotechnol.* **2017**, 12, 692–700.

3. Liu, L.H.; Guo, K.; Lu, J.; Venkatraman, S.S.; Luo, D.; Ng, K.C.; Ling, E.A.; Moochhala, S.; Yang, Y.Y. Biologically active core/shell nanoparticles self-assembled from cholesterol-terminated PEG-TAT for drug delivery across the blood-brain barrier. *Biomaterials* **2008**, 29, 1509–1517.
4. Qin, Y.; Chen, H.L.; Yuan, W.M.; Kuai, R.; Zhang, Q.Y.; Xie, F.L.; Zhang, L.; Zhang, Z.R.; Liu, J.; He, Q. Liposome formulated with TAT-modified cholesterol for enhancing the brain delivery. *Int. J. Pharm.* **2011**, 419, 85–95.
5. Rooy, I.; Mastrobattista, E.; Storm, G.; Hennink, W.E.; Schiffelers, R.M. Comparison of five different targeting ligands to enhance accumulation of liposomes into the brain. *J. Control. Release* **2011**, 150, 30–36.
6. Tzeng, S.Y.; Green, J.J. Therapeutic nanomedicine for brain cancer. *Ther. Deliv.* **2013**, 4, 687-704.
7. Trevaskis, N.L.; Kaminskas, L.M.; Porter, C.J. From sewer to saviour - targeting the lymphatic system to promote drug exposure and activity. *Nat. Rev. Drug Discov.* **2015**, 14, 781–803.
8. Swartz, M.A.; Hubbell, J.A.; Reddy, S.T. Lymphatic drainage function and its immunological implications: from dendritic cell homing to vaccine design. *Semin. Immunol.* **2008**, 20, 147–156.
9. Louveau, A.; Smirnov, I.; Keyes, T.J.; Eccles, J.D.; Rouhani, S.J.; Peske, J. D.; Derecki, N.C.; Castle, D.; Mandell, J.W.; Lee, K.S.; Harris, T.H.; Kipnis, J. Structural and functional features of central nervous system lymphatic vessels. *Nature* **2015**, 523, 337–341.
10. Mesquita, S.D.; Fu, Z.X.; Kipnis, J. The meningeal lymphatic system: a new player in neurophysiology. *Neuron* **2018**, 100, 375–388.
11. Mesquita, S.D.; Louveau, A.; Vaccari, A.; Smirnov, I.; Cornelison, R.C.; Kingsmore, K.M.; Contarino, C.; Onengut-Gumuscu, S.; Farber, E.; Raper, D.; Viar, K.E.; Powell, R.D.; Baker, W.; Dabhi, N.; Bai, R.; Cao, R.; Hu, S.; Rich, S.S.; Munson, J.M.; Lopes, M.B.; Overall, C.C.; Acton S.T.; Kipnis, J. Functional aspects of meningeal lymphatics in ageing and Alzheimer's disease. *Nature* **2018**, 560, 185–191.
12. Saad, W.S.; Prud'homme, R.K. Principles of nanoparticle formation by flash nanoprecipitation. *Nano Today* **2016**, 11, 212–227.
13. Zeng, Z.; Zhao, P.; Liu, L.; Gao, X.; Mao, H. Q.; Chen, Y. Lipid stabilized solid drug nanoparticles for targeted chemotherapy. *ACS Appl. Mater. Interfaces* **2018**, 10, 24969–24974.
14. Mei, L.; Rao, J.D.; Liu, Y.Y.; Li, M.; Zhang, Z.R.; He, Q. Effective treatment of the primary tumor and lymph node metastasis by polymeric micelles with variable particle sizes. *J. Control. Release* **2018**, 292, 67–77.
15. Cote, B.; Rao, D.; Alany, R.G.; Kwon, G.S.; Alani, A.W.G. Lymphatic changes in cancer and drug delivery to the lymphatics in solid tumors. *Adv. Drug Deliv. Rev.* **2019**, 144, 16–34.

16. Yaghini, E.; Turner, H.D.; Le Marois, A.M.; Suhling, K.; Naasani, I.; MacRobert, A.J. In vivo biodistribution studies and ex vivo lymph node imaging using heavy metal-free quantum dots. *Biomaterials* **2016**, 104, 182–191.

17. Reddy, S.T.; van der Vlies, A.J.; Simeoni, E.; Angeli, V.; Randolph, G.J.; O'Neil, C.P.; Lee, L.K.; Swartz, M.A.; Hubbell, J.A. Exploiting lymphatic transport and complement activation in nanoparticle vaccines. *Nat. Biotechnol.* **2007**, 25, 1159–1164.

18. Ryan, G.M.; Kaminskas, L.M.; Porter, C.J. Nano-chemotherapeutics: maximising lymphatic drug exposure to improve the treatment of lymph-metastatic cancers. *J. Control. Release* **2014**, 193, 241–256.

19. Saraiva, C.; Praça, C.; Ferreira, R.; Santos, T.; Ferreira, L.; Bernardino, L. Nanoparticle-mediated brain drug delivery: overcoming blood–brain barrier to treat neurodegenerative diseases. *J. Control. Release* **2016**, 235, 34–47.

20. Pardridge, W. M. CSF, blood-brain barrier, and brain drug delivery. *Expert Opin. Drug Del.* **2016**, 13(7), 963–975.

21. Nafee, N.; Youssef, A.; El-Gowelli, H.; Asem, H.; Kandil, S. Antibiotic-free nanotherapeutics: Hypericin nanoparticles thereof for improved *in vitro* and *in vivo* antimicrobial photodynamic therapy and wound healing. *Int. J. Pharmaceut.* **2013**, 458, 347–347.

22. Qian, C.; Yu, J.; Chen, Y.; Hu, Q.; Xiao, X.; Sun, W.;Wang, C.; Feng, P.; Shen, Q.D.; Gu, Z. Light-activated hypoxia - responsive nanocarriers for enhanced anticancer therapy. *Adv. Mater.*, **2016**, 28, 3313-3320.

Table of Contents

Nanoparticle delivery into the brain *via* the cerebral lymphatic vasculature is demonstrated by utilizing indocyanine green (ICG)-loaded PLGA nanoparticles as a model, bringing great opportunities for treating orthotopic glioblastoma and other central nervous system diseases.